Scale and space localization in the Kuramoto–Sivashinsky equation

Ralf W. Wittenberg[a] and Philip Holmes
Program in Applied and Computational Mathematics, Princeton University, Fine Hall, Washington Road, Princeton, New Jersey 08544

(Received 9 April 1998; accepted for publication 9 February 1999)

We describe a wavelet-based approach to the investigation of spatiotemporally complex dynamics, and show through extensive numerical studies that the dynamics of the Kuramoto–Sivashinsky equation in the spatiotemporally chaotic regime may be understood in terms of localized dynamics in both space and scale (wave number). A projection onto a spline wavelet basis enables good separation of scales, each with characteristic dynamics. At the large scales, one observes essentially slow Gaussian dynamics; at the active scales, structured ''events'' reminiscent of traveling waves and heteroclinic cycles appear to dominate; while the strongly damped small scales display intermittent behavior. The separation of scales and their dynamics is invariant as the length of the system increases, providing additional support for the extensivity of the spatiotemporally complex dynamics claimed in earlier works. We show also that the dynamics are spatially localized, discuss various correlation lengths, and demonstrate the existence of a characteristic interaction length for instantaneous influences. Our results motivate and advance the search for localized, low-dimensional models that capture the full behavior of spatially extended chaotic partial differential equations. © *1999 American Institute of Physics.* [S1054-1500(99)01902-3]

There has been much recent interest in the complex spatiotemporal behavior of extended systems with many degrees of freedom, which appear widely in applications. An important goal is to account for the dynamics of those energetically dominant modes in a spatiotemporally chaotic system, which occur at intermediate length and time scales, and to relate them to the dynamics observed (and understood via dynamical systems methods) in low-dimensional systems. In this paper, taking the Kuramoto–Sivashinsky equation as a model problem, we use wavelet decompositions to characterize spatiotemporal chaos, with a view to understanding dynamical interactions in space and scale and, thus equipped, to constructing low-dimensional local models.

I. INTRODUCTION

This work is motivated by the desire to understand the dynamics of coherent structures in fluid flows, whose interactions are, in many cases, responsible for turbulence production. These structures may be detected via the proper orthogonal decomposition (POD), or Karhunen–Loève decomposition, which is optimal in the sense of identifying the most energetic modes, on average. The dynamics, bifurcations and attractors of the low-dimensional dynamical systems obtained through Galerkin projection of the governing equations onto the POD modes then yield information on the localized interactions of coherent structures.[1–3]

The Kuramoto–Sivashinsky (KS) dynamics, visualized in Fig. 1 below, suggest the presence of structures having characteristic space and time scales and local dynamics. By analogy with the fluid case, we seek a reduced set of equations for the dominant modes on a suitable subdomain of $[0,L]$. However, for such spatially homogeneous systems with periodic boundary conditions, the POD modes are simply Fourier modes,[2] an observation which led to the proposal of localization via wavelet-based models.[4,5] The feasibility of such models was corroborated by the results that, compared to the POD (Fourier) basis, in a wavelet decomposition, little energy is lost on average,[4] and that suitably chosen low-dimensional wavelet projections can reproduce the essential small-L bifurcation behavior of the KS equation.[6]

We study the partial differential equation (PDE),

$$u_t + u_{xxxx} + u_{xx} + u u_x = 0, \quad x \in [0,L], \tag{1}$$

where $u_t \equiv \partial u/\partial t$, $u_x \equiv \partial u/\partial x$, and after rescaling the only control parameter is the system length L. Unless otherwise stated, we will consider periodic boundary conditions, and set the (conserved) spatial mean to zero. This equation has arisen in the context of several physical systems driven far from equilibrium by intrinsic instabilities, including plasma ion mode instabilities,[7,8] chemical phase turbulence,[9,10] flame front instabilities,[11] and fluctuations in liquid films on inclines.[12] Indeed, the KS equation may be generically derived as an amplitude equation near long-wavelength primary instabilities in the presence of appropriate symmetries.[13] In this paper we focus on the ''derivative,'' or conservation, form of the KS equation. For sufficiently large L, the solutions on the KS attractor display spatiotemporal chaos (STC), or ''weak turbulence,'' with a positive density of positive Liapunov exponents;[14] a typical evolution is shown in Fig. 1.

Our study of STC in the KS equation builds on numerous earlier studies via pointwise and Fourier statistics, nota-

[a]Current address: Institute for Mathematics and its Applications, University of Minnesota, 400 Lind Hall, 207 Church Street SE, Minneapolis, Minnesota 55455. Electronic mail: ralf@ima.umn.edu

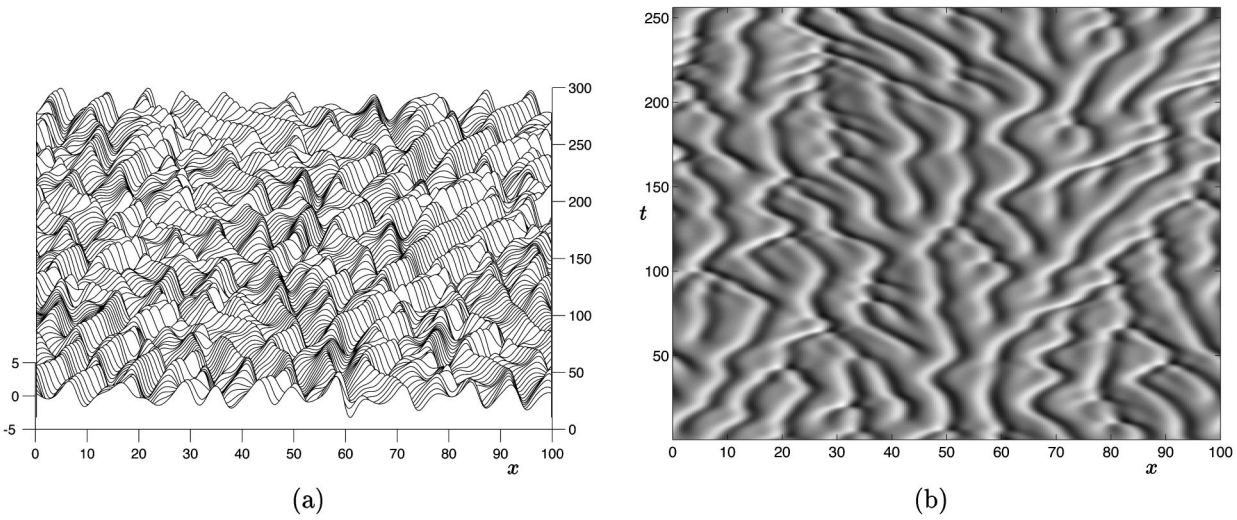

FIG. 1. (a) A solution of the KS equation (1) on the spatiotemporally chaotic attractor, for $L=100$, and covering 256 time units separated by $\Delta t=1$ (beginning at $t\approx 1.0\times 10^5$). (b) Gray-scale view of the evolution in (a), clearly showing the typical cellular structure, traveling cells, and creation and annihilation of peaks.

bly those of Pumir.[15] A review with many additional details and references appears in Ref. 16, particularly Chaps. 1 and 4, and here we merely indicate some key phenomena.

In Fourier space, we may write (1) with periodic boundary conditions as

$$\frac{d}{dt}\hat{u}_q=(q^2-q^4)\hat{u}_q+\sum_{q'} q'\hat{u}_{q'}\hat{u}_{q-q'}, \tag{2}$$

where $u(x,t)=i\Sigma_q\hat{u}_q(t)\exp(iqx)$, $q=2\pi n/L$, $n\in\mathbb{Z}$ (we will use q for the Fourier wave number throughout this paper to avoid confusion with the index k in the wavelet decomposition, Sec. II A). From the linear growth rate $\omega(q)=q^2-q^4=(2\pi n/L)^2[1-(2\pi n/L)^2]$, one sees that the uniform zero solution becomes unstable to the mode $n=1$ at $L=2\pi$. As L increases, the number of linearly unstable modes grows proportionately to L, with the most unstable mode at $q_0=1/\sqrt{2}$, or $n_0\in\mathbb{Z}$ near $L/2\pi\sqrt{2}$. The u_{xx} term is responsible for the instability at large scales; the dissipative u_{xxxx} term provides damping at small scales; and the nonlinear term uu_x (which has the same form as that in the Burgers or one-dimensional Navier–Stokes equations) stabilizes by transferring energy between large and small scales. For small L the dynamics are quite well understood;[17–19] intricate bifurcation diagrams describe transitions between families of steady states, traveling waves and more complex solutions. In particular, the small-L dynamics are characterized by the presence of modulated traveling waves and heteroclinic cycles.[19,20] For sufficiently large L (beyond about $L=50$ or 60), the ''simple'' solutions all become unstable to an (apparently unique) spatiotemporally chaotic attractor.[18]

It is readily confirmed that the KS equation (1) with periodic boundary conditions possesses the symmetries (i) $t\to t+\tau$ (temporal translation invariance); (ii) $x\to x+l$ (spatial translation invariance); (iii) $u(x,t)\to -u(-x,t)$ (parity); and (iv) $u(x,t)\to u(x-ct,t)+c$ (Galilean invariance). These symmetries are fundamental to the dynamics and bifurcation structure.[19,20] Individual solutions (Fig. 1) break these symmetries, but in the STC regime, they are restored in a statistical sense.

We study spatiotemporally chaotic dynamics in this regime by assuming the existence of a unique topologically transitive attractor, and invoking ergodicity to replace averages on the attractor by time averages along a single solution trajectory (checking that our results are independent of initial conditions, and that the integration time is sufficiently long for the statistics to converge). We appeal to the thermodynamic limit[21,22] $L\to\infty$ and the notions of extensive quantities (such as the energy) whose values are (asymptotically) proportional to L, and intensive quantities (for instance densities of extensive quantities) whose values are independent of the system size. A common interpretation[23] sees the large system as composed of interacting subsystems; in this view, extensive (proportional to the number of subsystems) and intensive (characteristic of a subsystem) quantities arise if interactions are spatially localized, so that the subsystems may be considered approximately uncorrelated for short enough times.

However, this picture is not rigorously established,[22] and even ''simple'' results on intensive properties, such as local pointwise bounds, remain unproven except for special solutions.[24,25] Such bounds would imply finiteness of the energy density $\epsilon(t)\equiv E(t)/L\equiv(1/L)\int_0^L u^2(x,t)dx$ in the limit $L\to\infty$, as numerical solutions suggest, but the best available bounds[26] give $\limsup_{t\to\infty}\epsilon(t)\leqslant cL^{11/5}$. Similarly, while solutions are known to be analytic,[27–29] their decay rate has not been shown to be L-independent.

The conjectured existence of a finite energy density and width of the analyticity domain in the large-L limit is consistent with the calculated energy (or power) spectrum (Fig. 2), which is well known.[30–32] The normalized spectral density $S(q)\equiv L\langle\hat{u}_{-q}\hat{u}_q\rangle$ appears independent of L in the complex regime (Fig. 2), indicating an invariant distribution of

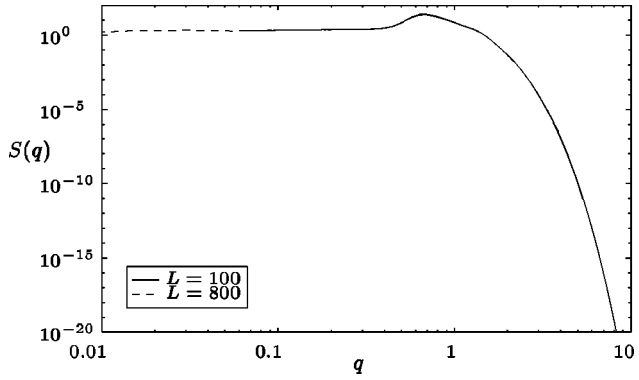

FIG. 2. Rescaled power spectrum $S(q)$, for $L=100$ and $L=800$.

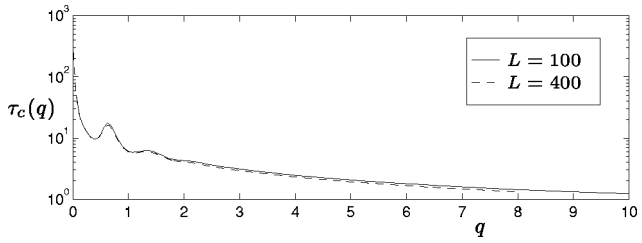

FIG. 3. Correlation times $\tau_c(q)$ for different Fourier modes $\hat{u}_q(t)$.

energy among the Fourier modes in the thermodynamic limit. The power spectrum is basic to understanding the KS statistics and dynamics, and we shall frequently refer to it in the following. Many of its properties have been accounted for,[31] and its general shape modeled;[32] we summarize the main features:

The exponential tail is due to the strong dissipation at *small* scales, corresponding to the exponential decay of the Fourier modes of an analytic function. The *active* scales contain most of the energy, with a pronounced peak at $q=q_m \approx q_0=1/\sqrt{2}$, corresponding to a characteristic length $l_m = 2\pi/q_m$; that is, it turns out that the most linearly unstable mode *approximately* coincides with the peak of the energy spectrum in the nonlinear system (our calculations suggest that q_m is slightly less than q_0; the nonlinearity induces a shift to larger scales). Within the active region, it is remarkable that for $0.8 \lesssim q \lesssim 1.25$, there is a definite power law decay with an exponent experimentally indistinguishable from 4.0; by analogy with the inertial range in fluid turbulence, it is tempting to think of this region $S(q) \sim q^{-4}$, where production and dissipation are almost balanced ($q^2 \approx q^4 \approx 1$), as an ''inertial range.''[31] In the *large* scale region, there is a shoulder which flattens as $q \to 0$, reminiscent of a thermodynamic regime with equipartition of energy.

The chaotic dynamics at the active and small scales simulate the effect of random forcing on the largest scales, so that the scaling of solutions for low q is well described by a forced Burgers, or Kardar–Parisi–Zhang (KPZ) equation,[33–35] with a positive effective viscosity; in particular, this asymptotic description predicts a flat spectrum, $S(q) \to$ const as $q \to 0$. There has been considerable effort towards making this more precise, both numerically[36] and analytically;[37] a central result of this work is the existence of a crossover to asymptotic KPZ scaling for lengths $L \sim 4000$, beyond which the predicted scaling has been observed. Here we do not consider lengths approaching the crossover to KPZ scaling, however; we focus on the STC dynamics in the active regime, with $q=\mathcal{O}(1)$. As we show in Sec. II below, the three regimes—large-scale (thermodynamically equilibrated), active intermediate, and damped small-scale—are well separated, and may be characterized independently; and we do not believe that the crossover in the dynamic scaling at very large scales affects the properties of STC at the $\mathcal{O}(1)$ scale of the characteristic ''cellular'' structures.

Concerning temporal behavior, the (spatially averaged) temporal autocorrelation function $c(t)$ yields an autocorrelation time $\tau_c \approx 10$ from the width at half-maximum of the peak of $c(t)$. We find that this characteristic time between ''events'' τ_c remains essentially constant with increasing L in the STC regime, showing that it is an intensive property of the dynamics in the large-L limit. The temporal behavior is strongly scale-dependent, however, as revealed by the autocorrelation times $\tau_c(q)$ of the spatial Fourier modes $\hat{u}_q(t)$ (Fig. 3). The small-scale dynamics are rapid, with a characteristic time which appears to decrease as a power law, while the slow large-scale dynamics show divergence of $\tau_c(q)$ as $q \to 0$.

Near the peak of the power spectrum, $q_m \approx q_0$, there is a pronounced local maximum in $\tau_c(q)$ for q near q_m, with a correlation time $\tau_c(q_m) \approx 18$, somewhat larger than the characteristic time τ_c for the field u as a whole. In this active region, a faster linear growth rate is correlated with slower dynamics. We believe that the longer time scales for the excited modes arise from the metastability of the cellular solutions (which are stable for small L) undergoing continuous creation and annihilation events (''space–time defects'').[38]

Most of the long-time statistical computations presented here were performed by integration of (2) with a Fourier pseudospectral method, keeping modes up to at least $q_{\max} \geqslant 4$, integrating the linear terms exactly and using an Adams–Bashforth time-stepping scheme for the nonlinear terms. For N equations, this method requires $\mathcal{O}(N \log N)$ iterations per time step. Results were also obtained and checked with an $\mathcal{O}(N)$ combined Crank–Nicholson/Adams–Bashforth finite difference solver for (1), second order in x and t, with a typical space step $\delta x = 100/256 \approx 0.39$. Typical time steps were $\delta t = 0.0625$ and 0.03125, and averaging was performed over samples separated by $\tau = 0.25$. The quantitative results were checked with smaller space and time steps, and more Fourier modes; the results presented are well-converged.

The remainder of this paper is organized as follows: After introducing the wavelet decomposition, in Sec. II we show that this representation provides good scale separation leading to better understanding of the STC in terms of characteristic dynamics at different scales. In particular, the statistics of the intermediate energetic scales correspond to local events observed for low-dimensional systems. This STC scale separation is qualitatively invariant under changes in

the length of the domain. The existence of a characteristic length scale of the dynamics is shown in Sec. III, and further studied and exploited in novel numerical experiments in which interactions between separated spatial domains are cut; this provides a basis for the hypothesis of the extensivity of the KS dynamics—that the large system behaves essentially as a union of smaller, spatially localized subsystems—and motivates our continuing search for low-dimensional local models. Section IV contains a brief discussion.

II. WAVELET DECOMPOSITION AND SCALE LOCALIZATION

The Fourier spectral results presented in the previous section enable us to study the behavior at different ranges of scales. However, all Fourier-based properties (such as the energy spectrum and time correlations) are continuous in q; there is no separation of scales. For some purposes we might prefer to group ranges of Fourier modes to separate and distinguish properties local to these ranges. Also, each Fourier basis function is uniformly supported on the entire spatial domain, so that this representation is unable to capture any properties that arise from spatial localization. The phase relationships between different Fourier modes, which give rise to spatially local features in the superposition, are lost in the averaging which gives the power spectrum and statistics. This motivates the use of a spatially localized basis, which may be able to detect dynamic features arising from concentrated events; wavelets appear well-suited for this purpose.

A. The wavelet decomposition

Our study of KS dynamics using a basis localized in both space and scale is based on the familiar multiresolution analysis and orthogonal wavelet decomposition; see Refs. 39, 40. In highlighting the main features needed below, we largely follow Elezgaray *et al.*[41]

The construction of the orthonormal wavelet basis begins with a suitably chosen function $\Psi(x)$, satisfying appropriate technical conditions,[39] and normalized so that $\int_{-\infty}^{\infty}\Psi^2(y)dy=1$. The set of functions $\{\tilde{\psi}_{jk}(y), j\geqslant 0, k=0...2^j-1\}$ built by dilation and translation of $\Psi(y)$, and periodization,

$$\tilde{\psi}_{jk}(y)=\sum_{n\in\mathbb{Z}} 2^{j/2}\Psi(2^j(y+n)-k),\quad y\in[0,1], \tag{3}$$

then forms an orthonormal basis for zero mean, finite energy periodic functions on $[0, 1]$ (the scaling function at the coarsest scale $j=0$ vanishes due to the zero mean condition). We then obtain an orthonormal basis $\{\psi_{jk}\}$ on $[0,L]_{\text{per}}$ simply by rescaling $\psi_{jk}(x)=L^{-1/2}\tilde{\psi}_{jk}(x/L), x\in[0,L]$. From the symmetry of $\Psi(y)$ about $y=1/2$, $\psi_{jk}(x)$ is centered about $x_{jk}=L2^{-j}(k+1/2)$. We shall frequently use α to denote the multi-index (j, k).

It follows from the definition (3) that varying j (which we will refer to as changing the wavelet ''level'') allows one to ''zoom in'' or ''zoom out,'' while changes in k correspond to horizontal translations. By our choice of convention, $j=0$ refers to the largest scale; more generally, small j implies large, or coarse, scales, while large j indicates small, or fine, scales.

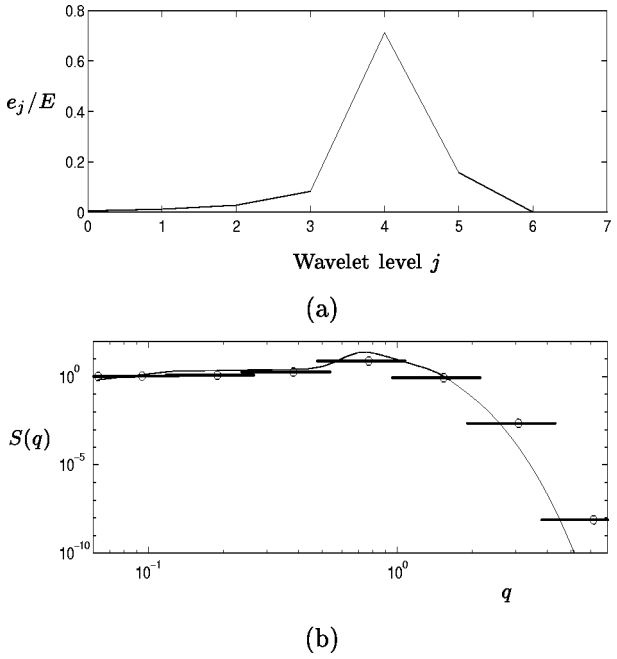

FIG. 4. (a) Fraction of time-averaged total energy, $\langle e_j(\cdot)/E(\cdot)\rangle$, as a function of wavelet level j, for $L=100$. (b) Power spectrum $S(q)$ (Fig. 2), compared to the energy per individual wavelet at each level j. The wavelet distribution is plotted with the center and range of 99% of the support in Fourier space.

The usefulness of the wavelet decomposition follows from the relatively localized support of Ψ (and hence of the ψ_α) in both real and Fourier space (of course, by the uncertainty principle, one cannot achieve complete localization in both x and q). Following Refs. 4–6, 41 we have chosen to use an orthonormal, periodic spline wavelet basis,[42] based on the Battle–Lemarié construction of mth order spline wavelets (see Ref. 39). These wavelets are of class C^{m-2}, and have the properties of $m-1$ vanishing moments, exponential decay in x, and algebraic decay in q as $|q|\to 0$ and $|q|\to\infty$. Increasing m improves the smoothness and localization in q, at the cost of increasing the spatial support of the wavelet; we expect to need at least four derivatives for ψ to capture the behavior of the u_{xxxx} term in the KS equation (1) satisfactorily. In this paper we have used $m=8$, and checked our results with $m=6$; see for instance Ref. 16, Fig. 3.1 and Ref. 6, Fig. 1 (for $m=6$) for examples of these spline wavelets.

In the following we use the wavelet decomposition of the solution $u(x,t)$ of the KS equation,

$$u(x,t)=\sum_{j=0}^{J}\sum_{k=0}^{2^j-1} a_{jk}(t)\psi_{jk}(x)\equiv\sum_{\alpha} a_\alpha(t)\psi_\alpha(x) \tag{4}$$

(as in Fourier representations, a suitable cutoff J is justified by the small-scale exponential decay of the solution; see for instance Fig. 4). The quantities of interest to us are then the time-dependent wavelet coefficients $a_{jk}(t)$, which reveal the behavior of $u(x,t)$ at level j and position given by k. In the

remainder of this section, we study the statistics, including temporal behavior and distributions, of these wavelet coefficients.

B. Wavelet analysis: Energy distribution and temporal behavior

In this section, we will present results for the KS evolution for $L=100$, a typical length well in the STC regime, but still short enough to allow sufficiently fast calculations and well-converged statistics; we shall briefly discuss the dependence on L below. For $L=100$, the peak of the Fourier spectrum is at $q_m \approx q_0 = 1/\sqrt{2}$, or at $n_m = q_m L/2\pi \approx 10.7$, and the highest unstable mode is at $L/2\pi \approx 15.92$. That is, there are 16 complex, or 32 real linearly unstable or marginal modes, and the energy is concentrated in the neighborhood of the 22nd real mode. Hence the peak is located in wavelet level 4 (levels 0–3 contain a total of $\Sigma_{j=0}^{3} 2^j = 15$ modes).

As a guide to later calculations, we compute the energy in each wavelet level [since $\{\psi_{jk}\}$ is an orthonormal basis, this is simply found from $e_j(t) = \Sigma_k a_{jk}^2(t)$]. Figure 4 shows the time averaged energy per wavelet level, as well as the energy for each individual wavelet at that level, given that there are 2^j wavelets at level j (by translational invariance, all wavelets at a given level have identical statistics). Comparison of Fig. 4(b) with the power spectrum in Fig. 2 shows a similar distribution of energy per mode, confirming that the wavelets are well-localized in Fourier space. In the dissipative range, the wavelet energies decay more slowly than $S(q)$, however; this arises largely because each wavelet level overlaps a range of Fourier modes, and with exponentially decaying power spectrum, the wavelet energies are strongly weighted by the low-q end of the range.

From Fig. 4(a), we can identify the levels with distinct behaviors. Wavelet levels 0, 1, and 2 correspond to large scales, containing a small fraction (under 5%) of the total energy, due especially to the small numbers of wavelets at these scales—this corresponds to the nearly flat region of the Fourier spectrum. Levels 3, 4, and 5 contain the active, energetic modes near the peak of the Fourier spectrum, and together account for over 95% of the energy distribution. Levels 6, 7, and any higher (smaller scale) levels, with less than 0.1% of the energy, are strongly damped, with exponentially decreasing energy in the dissipative range.

Typical time series for wavelet coefficients at each level (for wavelets at each scale centered near $x=L/2$, taken for the same time interval) are shown in Fig. 5. From this, we can clearly see the differences in time scales, distributions, and dynamics at the different scales. Characteristic times τ_j for each level j are shown in Fig. 6 (compare Fig. 3).

C. Probability distributions of wavelet coefficients

In Fig. 7 we show the probability distribution functions (PDFs) for the wavelet coefficients at each level, averaged over time, and over the 2^j wavelets at each level j (compare Ref. 41, Fig. 1). This figure is one of the main new results of this paper, and clearly shows how the wavelet representation reveals both scale and spatially localized information.

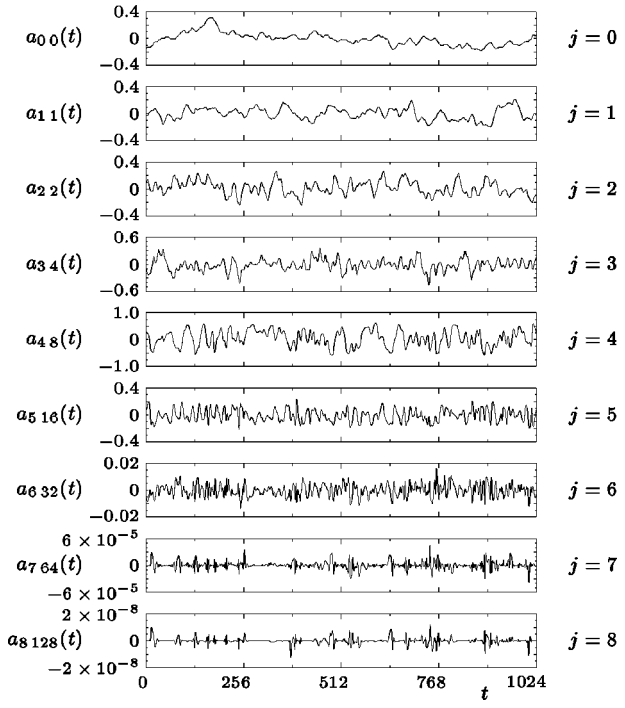

FIG. 5. Sample time series for one wavelet coefficient $a_{jk}(t)$ at each level j, for $k=2^j/2$, that is, centered near the middle of the domain of length $L=100$.

For large scales, the distributions are Gaussian. At these scales, the support of each wavelet includes several characteristic wavelengths. Due to spatial decorrelation and independence of sufficiently separated positions (Sec. III B), the averaging over several characteristic structures inherent in the large-scale wavelet coefficients may thus be expected to lead to the normal distribution. At the coarsest scales, therefore, the dynamics resemble slow noise. These results are motivated from a different perspective from the existence of a fluctuation-dissipation theorem for the one-dimensional forced Burgers equation,[35,43] which implies that the field u obeys a Gaussian distribution at large scales, in the KPZ limit. Note that the PDFs for the lowest j values are less well converged; this is both due to the fact that there are fewer wavelets at these j, over which to average; and also because the dynamics at the large scales are slow, requiring more time for statistical equilibration (see Figs. 5 and 6).

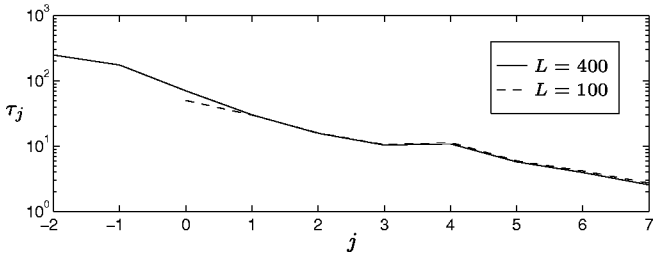

FIG. 6. Mean-square autocorrelation times τ_j for the time series of wavelet coefficients at different scales j. Note that the values for $L=400$ are shifted by two wavelet levels (we plot, in fact, τ_j against $j-2$). Compare Fig. 3, noting that the horizontal axes are logarithmically related to each other ($j \propto \log q$).

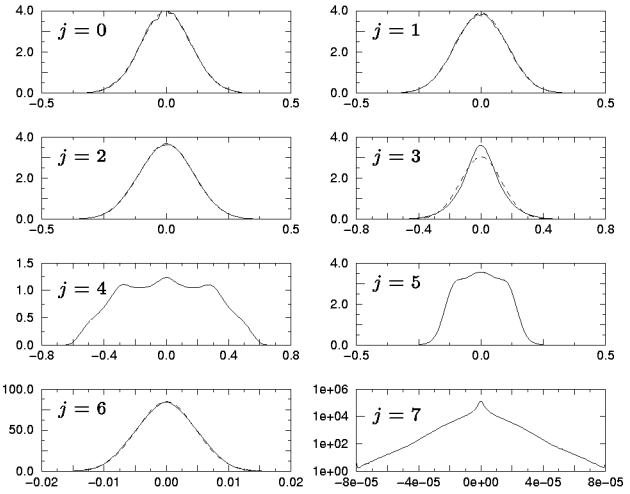

FIG. 7. Probability density functions for the wavelet coefficients at each level $j=0,...,7$, for $L=100$. For $j=0-3$ and 6, a best-fit Gaussian distribution is superposed. Note the logarithmic axis for $j=7$, denoting a near-exponential distribution.

At the energetic scales $j=3$, 4, and 5, the support of the wavelets is comparable to the characteristic intrinsic wavelength $l_m=2\pi/q_m$, and the PDFs are quite different, displaying features unlike any observed in the Fourier representation. The $j=3$ level, although still largely in the flat part of the Fourier spectrum, shows a distinct steepening of the distribution relative to a Gaussian. Levels 4 and 5 show the most striking, nonequilibrium PDFs, comparable to the distributions for local values of u:[44] A broad, triple-humped distribution, superposing a peak at 0 and a double-humped peak reminiscent of the cellular (sinusoidal-like) solutions. This is most striking at $j=4$, which contains the most energetic modes and the characteristic length l_m, but $j=5$ also shows this behavior. Unlike the Fourier coefficient distributions, the wavelet coefficients appear to capture on average the spatially local structures and events at the active scales.

The PDF for level $j=6$ is again well fitted by a Gaussian; it is interesting that such an equilibrium distribution should appear well within the dissipative range, possibly via some balance between energy fed in from adjacent active scales, and dissipation. Indeed, computation of the Fourier global energy flux confirms that there is fairly significant energy transfer over the range of scales covered by $j=6$.

At the smaller scales, $j\geqslant 7$, the effects of strong dissipation are apparent. The amplitudes a_{jk} decay exponentially with j in this regime, while the distributions have super-Gaussian tails. That is, the small scale coefficients remain near zero most of the time, with occasional (intermittent) excursions of relatively large amplitude driven by events at larger scales; for instance, note the ''event'' beginning near $t=256$ at level $j=7$, one of several visible in Fig. 5, which appears to be driven by activity in levels $j=5$ and 6, and entrains a similar, though smaller, excursion in an adjacent $j=8$ wavelet. The near-exponential PDF is reminiscent of those observed for velocity increments and gradients, which signal intermittency in turbulence;[45] good fits to such turbulent PDFs have been obtained in some models.[46,47] In fact, recalling that the wavelet transform at small scales acts as a high pass filter, our observed small-scale behavior is closely related to turbulent dissipation-range intermittency, seen when the velocity field is filtered at a frequency associated with a scale comparable to the Kolmogorov dissipation scale;[45] Frisch and Morf[48] showed that infrequent bursts leading to intermittency are associated with singularities at complex times of time-analytic functions u (such functions include solutions of the KS equation[29]).

An alternative view of the small-scale PDF derives from the properties of the wavelets; if at the scale of the analyzing wavelet, the field u is locally linear, or more generally a low-order polynomial, then by the low-order moment cancellation property of these smooth wavelets,[39] the corresponding wavelet coefficient vanishes. Thus the small-scale wavelets will have non-negligible coefficients only where $u(x,\cdot)$ has large curvature, that is, where there is a peak or trough of the field u. That is, the small-scale dynamics track the positions of the ''coherent structures.''

We note that the scale separation afforded by the wavelet decomposition depends on the interplay between wavelet and intrinsic length scales, specifically, on the distances $l_j=L2^{-j}$ between the centers of adjacent wavelets at level j in the dyadic wavelet decomposition, and the characteristic length l_m of the dynamics. Consequently, we expect that as L varies, there is a shift in the distribution of energy among wavelet modes, and in the coefficient PDFs at different levels. The statistics in this paper are presented for $L=100$, but computations for other lengths (see Ref. 16) confirm that these results, for instance those of Fig. 7, are not special; a comparison with $L=80$ and $L=128$ shows that while the detailed form of the PDFs may change, the characteristic separation of scales and distinction between the distributions for large, active, and small scales is retained throughout the STC regime. Furthermore, comparing distributions for $L=100$ and $L=400$ verifies that a change in L by a power of two corresponds to an integral shift in the wavelet levels, the PDFs otherwise remaining invariant; this confirms that our $L=100$ results are well-converged ''large-L'' statistics in the STC regime. It is plausible that there is a continuous distribution of density functions, interpolating between those shown, so that for each L, a discrete subset is selected.

D. Scale-by-scale structure of the dynamics

A projection of the solution onto a wavelet basis thus clearly allows us to distinguish between average behavior of the dynamics at different wavelet levels; the major features are large-scale randomness, small-scale intermittency, and distributions reminiscent of characteristic events in intermediate active scales (creation and annihilation of peaks, and traveling waves with a typical intermediate wavelength). We have attempted heuristic justifications for these PDFs, and hope for a theoretical derivation of some of these results from the underlying KS equation. We now show how wavelets may be used as an experimental tool, explicitly probing the dynamical significance of wavelet levels to obtain a detailed picture of how different scales contribute to the overall dynamics.

We perform these experiments by overwriting modal co-

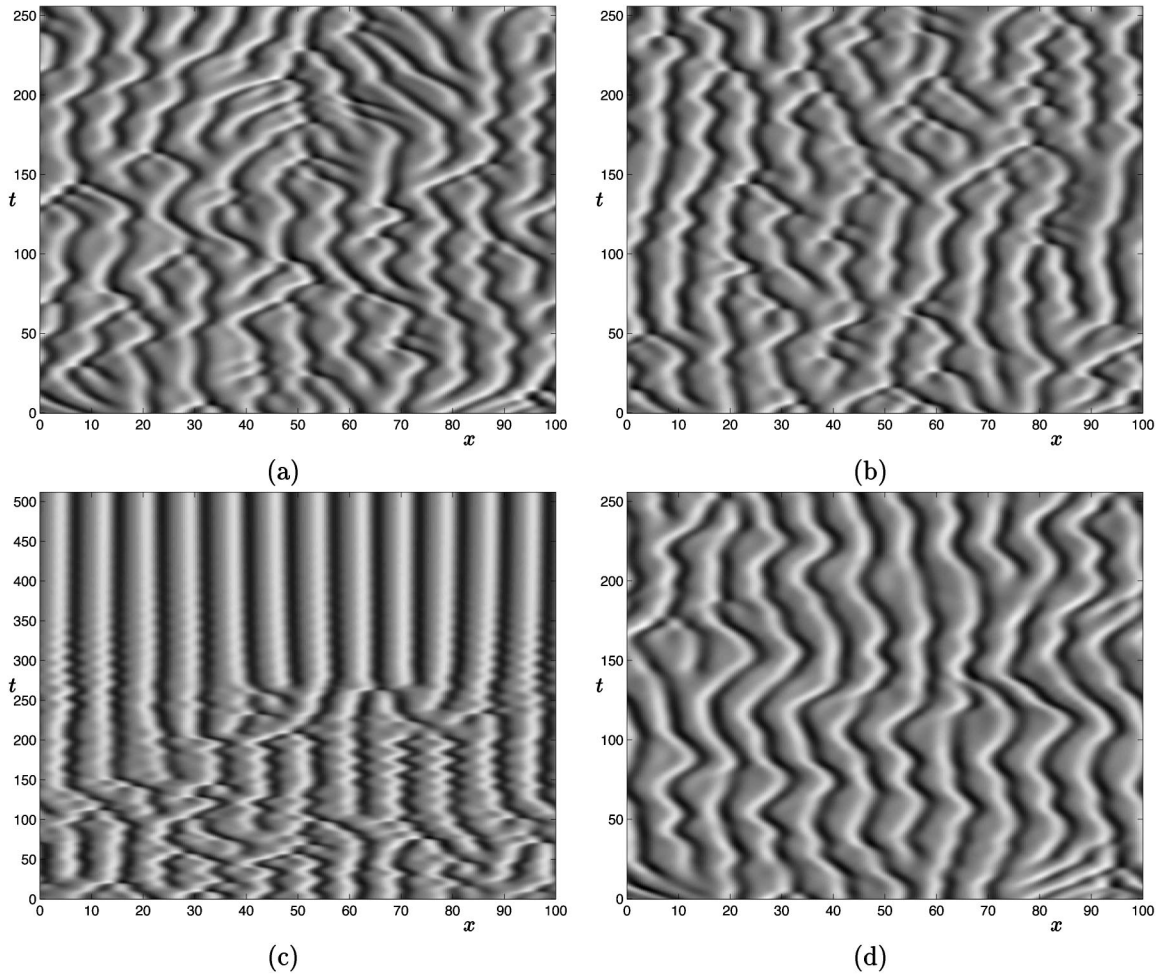

FIG. 8. The scale-by-scale structure of the dynamics, elucidated by setting various wavelet levels to zero. Levels eliminated (a) $j=0$; (b) $j=0$ and 1; (c) $j=0$, 1, and 2 (note the change of time scale); (d) $j=3$.

efficients at each time step. Specifically, we integrate the full KS equation for the wavelet modes $\{a_{jk}\}$ using a wavelet pseudospectral solver. We then eliminate, say, wavelet level j by setting all the modes at that level to zero after each time step; similarly, we can force at particular modes by replacing them with values computed from independent runs or via a model of some kind (see Ref. 49 for a similar approach to the investigation of two-dimensional Navier–Stokes dynamics). By successively eliminating or driving different levels or combinations of levels, we may thus discern their respective contributions to the spatiotemporally chaotic dynamics. As before, we confine our discussion to $L=100$, for which Fig. 7 summarizes the distinctions between levels.

From the results of numerous such experiments, described more fully in Ref. 16, Chap. 5, we find that the small scale levels $j\geqslant 6$ are essentially irrelevant to the dynamics, as they are slaved to the larger scales; their elimination has little effect except on detailed (pointwise) tracking. The most energetic active scales, $j=4$ and 5, responsible for most of the characteristic spatial structure, are crucial; removal of either or both of these levels results in rapid finite-time blowup of the simulation, showing that they are basic to the energy transfer and dissipation mechanism stabilizing the larger scales.

The most revealing results of these experiments occur at the largest scales. Figures 8(a)–8(c) shows the effect of successively ''turning off'' levels 0–2, demonstrating that they serve to maintain disorder without being essential to the energy balance. Eliminating level 0 has little effect [Fig. 8(a)], while in (b), we see that without levels $j=0$ and 1, the dynamics are slightly more rigid, and closer to a cellular state than for the full KS equation [Fig. 1(b)]. In the absence of all the large scales with Gaussian distributions (Fig. 7), $j=0$, 1, *and* 2, there is some (transient) dynamical activity, but eventually the solution collapses to a stationary cellular (roll) state, reminiscent of the attractor for some small L values[18,50] [Fig. 8(c)]. Recalling Fig. 4(a), observe that this drastic effect on the dynamics is the consequence of removing modes containing less than 5% of the total energy. These experiments thus demonstrate explicitly the role of the large scales, $j\leqslant 2$ for $L=100$, in contributing the excitation which drives the active scales $j\geqslant 3$ and maintaining persistent disorder in the STC regime. (Note that level 2 is not essential for this

purpose; in the absence of $j=2$, levels 0 and 1 can maintain disorder.)

The picture of the large scales driving the dynamics through a noisy ''heat bath'' is consistent with their Gaussian PDFs and with the forced Burgers equation description of the effective large-scale dynamics. On the other hand, the KS equation is completely deterministic, and we might conceivably expect the characteristic KS dynamics to depend on correlations between the large- and active-scale modes. We have tested the hypothesis that the dynamical significance of the large scales is solely due to their Gaussian nature, without regard to their deterministic origins, by forcing at levels $j \leqslant 2$ with an autonomously generated stochastic process [Ref. 16, Sec. 5.5.2]. Specifically, we have used a modified Ornstein–Uhlenbeck process (Langevin equation with colored noise), with parameters obtained from the effective forced Burgers description of the large-scale dynamics;[44] this process reproduces the large-scale statistics extremely well. When the modes at wavelet levels $j=0$, 1, and 2 are each driven independently by such a process, the remaining levels undergoing KS dynamics, the resulting evolution is visually and statistically remarkably close to that of the full KS equation. That is, purely stochastic large-scale evolutions appear to have the same effect as their deterministically derived counterparts in the way they drive chaotic dynamics at the active scales; the dynamical contributions of the large scales in the KS equation are essentially random.

In Fig. 8(d), we see an experiment in which level $j=3$ is eliminated (recall its strongly peaked distribution, Fig. 7). As seen in the figure, without this intermediate level, there are fewer typical creation and collision events; rather, the dynamics are dominated by the relative enhancement of cellular structures undergoing (modulated) traveling-wave-type behavior. Level 3 thus appears to play a major role in driving the distributions towards zero, and in maintaining the ''events,'' the dynamical interactions of coherent structures, and defect generation and annihilation, characteristic of the STC state. These conclusions are supported by experiments in which both levels $j=2$ and 3 are removed. Observe also that these experiments, and similar ones, show that the largest scales can drive the active scales even in the absence of intermediate levels; that is, nonlocal energy transfer in scale occurs.

We have summarized a series of experiments in which we actively intervene in the system, manipulating different wavelet levels, to discern the scale-by-scale structure of the STC regime. Extensive experiments in which other modes are eliminated, or forced from an external run or otherwise, are reported in Ref. 16, and confirm the above conclusions. The wavelet representation thus provides a detailed dynamical picture, enhancing the insights obtained from the averaged distributions, of the spatiotemporally complex dynamics viewed as arising from the interactions of distinct and complementary contributions of different scales.

III. SPACE LOCALIZATION

In the attempt to characterize homogeneous STC, much attention has been focused on finding relevant measures of spatial localization (see Ref. 21, pp. 945ff or Ref. 22). The existence of intrinsic correlation lengths is fundamental to the concept of ''extensive chaos'' and a thermodynamic limit—if interactions are spatially localized, then in the interpretation of the ''very large'' system in terms of coupled, sufficiently large subsystems, we do not expect ''new'' global collective effects to emerge as the number of these coupled subsystems increases as $L \to \infty$.

From the point of view of (instantaneous) dynamics, we are interested in the role of spatial localization in determining the ''typical events'' of Fig. 1, such as local stretching and compression of cells, and creation and annihilation of peaks. Furthermore, to aid the search for low-dimensional models representing the dynamics of a few localized modes in a short system, we would like to obtain a characteristic length as an indication of the size of small system required for successful modeling.

A. Boundary conditions

Throughout this paper we have considered the translationally invariant KS equation (1) with periodic boundary conditions. This ensures that the dynamics observed are intrinsic to the KS equation (hence expected to persist in the thermodynamic limit), and not driven or influenced by the boundary. A measure of spatial localization is the independence of bulk dynamics of the boundary conditions, and the width of the boundary layer gives an estimate of the interaction distance. Thus in this brief section only, we consider the effects of fixed, nonperiodic boundary conditions; in which case, the behavior at least near the walls is strongly constrained by the boundary. However, as we see in Fig. 9 (compare Fig. 1), even for fixed (either rigid, $u=u_x=0$ at $x=0$, L, or Dirichlet, $u=u_{xx}=0$ at $x=0$, L) boundaries, for sufficiently large L the characteristic spatiotemporally chaotic KS dynamics are observed in the bulk of the domain; sufficiently far from the boundaries, the system ''forgets'' its boundary conditions. In addition to visual inspection of space–time plots [Figs. 9(a) and 9(b)], the decay of boundary influences is observed in the moments of the pointwise distributions as a function of distance from the boundary,[15] in the mean profile for rigid boundary conditions[51] [Figs. 9(c) and 9(d)], and in the lack of dependence of bulk correlation times on boundary conditions (Egolf and Greenside[51] have argued that for rigid boundary conditions, correlation times are x-dependent even far from the boundary, but it appears that this result is an artifact of the root-mean-square width method they use to calculate the correlation time; see Ref. 16). In each case, the dynamics appear to settle down to their bulk values beyond a boundary layer of width $l_b \sim 20-25$. [We note however from Figs. 9(a) and 9(c) that rigid boundary conditions induce a slight overall tilt on the mean profile $m(x)$, and a preferred drift to the left; see Ref. 52.] This provides further evidence of spatial localization of the dynamics, and absence of significant interactions beyond some characteristic interaction length.

B. Correlation lengths

Returning to periodic boundary conditions, there are many possible choices for an appropriate correlation length

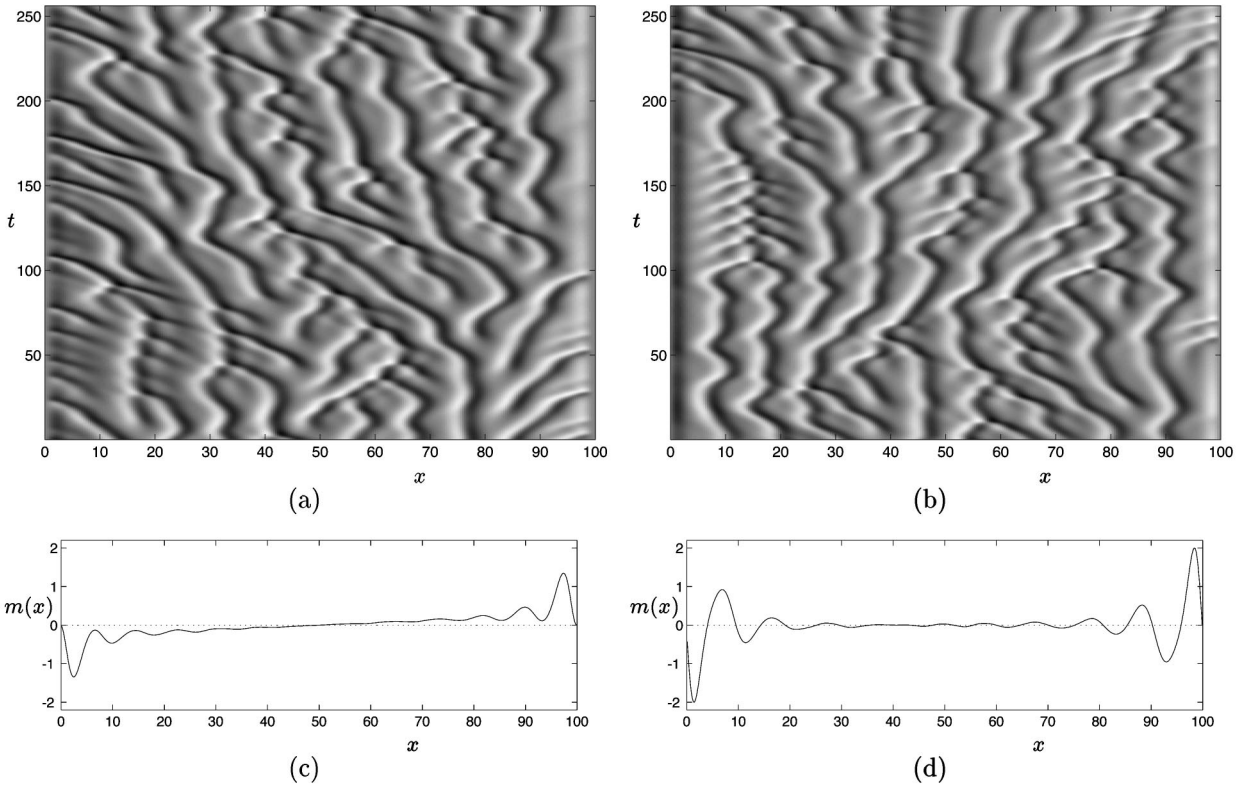

FIG. 9. Effect of boundary condition variations. (a) Rigid boundary conditions $u=u_x=0$; (b) Dirichlet boundary conditions $u=u_{xx}=0$. Time-averaged, space-dependent mean profiles $m(x)\equiv\langle u(x,\cdot)\rangle$ for (c) rigid, (d) Dirichlet boundary conditions.

for STC,[21,22] and it is not yet clear which are the most relevant. In this section we discuss some of the candidate length scales for our system, and then describe an experiment designed to elucidate a *dynamic* interaction length. Any correlation length should, *a priori*, be constructed out of the two lengths in our equation, the system length L and the most excited Fourier wavelength $l_0=2\pi/q_0$; and we expect that extensivity implies that correlation lengths are asymptotically independent of L.

Two of the simplest length scales which measure spatial disorder and localization are the two-point correlation length ξ_2 and the mutual information correlation length ξ_I. We compute the spatial single-time autocorrelation function $C(x)=\langle u(x',t)u(x'+x,t)\rangle$ (independent of x' by spatial homogeneity) from the inverse Fourier transform of the power spectrum of Fig. 2; its invariance under L follows from that of the power spectrum $S(q)$. As shown in Fig. 10, the correlation function is well modeled by the functional form $C(x)\approx C(0)\cos(q(x))\exp(-x/\xi_2)$, where to lowest order $q(x)\approx\tilde{q}x$, with $\tilde{q}$ near the peak of the power spectrum. The correlation function thus captures both the underlying oscillatory, cellular spatial structure of the KS dynamics, and the rapid spatial decorrelation reflecting the spatial disorder in the STC regime. An improved fit to $C(x)$ for reasonably small x, shown in Fig. 10(b), is given to quadratic order by $q(x)\approx 0.75x-0.005x^2$; the resulting two-point correlation length is $\xi_2\approx 7.4$. As measured by the two-point correlations, spatial coupling becomes negligible beyond a few multiples of ξ_2.

The autocorrelation function $C(x)$ depends only on $\langle|\hat{u}_q|^2\rangle$, and as such is a linear measure of interactions; we might expect a quantity which depends nonlinearly on the dynamics to capture additional features.[53] The independence of two spatial locations in the KS equation, or of two time series $s_1(t)$ and $s_2(t)$ more generally, may be quantified by the mutual information I,[54,55] which measures the average

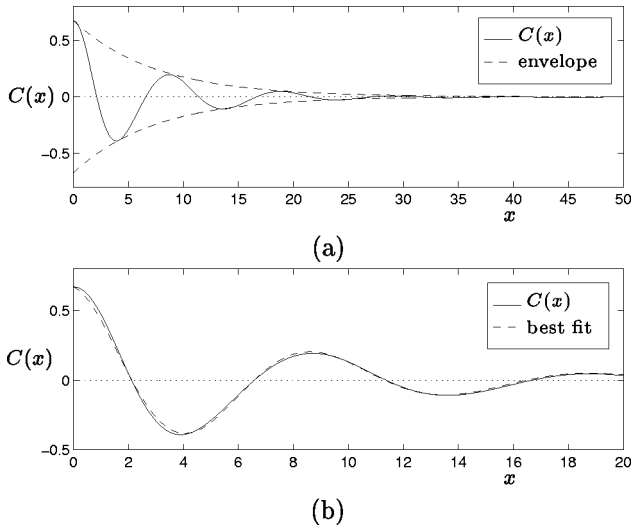

FIG. 10. (a) Spatial autocorrelation function $C(x)$ for $L=100$, with exponential envelope $C(0)\exp(-x/\xi_2)$. (b) Enlargement of (a), with best fit $C(0)\cos(q(x))\exp(-x/\xi_2)$, taking $q(x)$ to quadratic order.

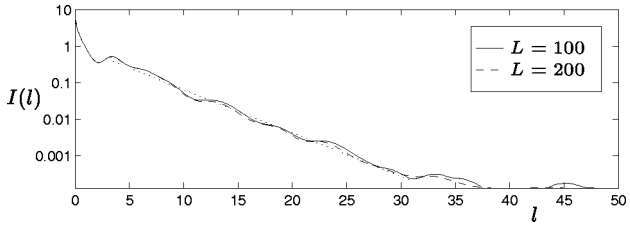

FIG. 11. The mutual information $I(l)$; the dotted line is a fit to the $L=200$ data, showing the exponential decay over a correlation length $\xi_I \approx 3.8$.

amount of information about s_1 contained in s_2, or more specifically, the average reduction in the entropy of $s_1(\cdot)$, given knowledge of $s_2(\cdot)$. Given a discrete partition $\{S_i\}$ of the state space for $s_1(\cdot)$, with probabilities p_i, and similarly, probabilities q_i for $s_2(\cdot)$ and a joint probability distribution r_{ij} for s_1 and s_2, the mutual information may be estimated by

$$I(s_1(\cdot),s_2(\cdot))=\sum_{i,j} r_{ij}\log_2\frac{r_{ij}}{p_i q_j}. \tag{5}$$

In the context of chaotic dynamics, a mutual information correlation time was proposed by Fraser and Swinney[56] as an optimal estimate for the choice of delay time for the reconstruction of attractors from time series.

For our application, to test the asymptotic independence of two spatial locations separated by l, we compute $I(l) \equiv I(u(x,\cdot),u(x+l,\cdot))$ (averaged over x, by appeal to homogeneity). In this case, the distributions p_i of $u(x,\cdot)$ and q_i of $u(x+l,\cdot)$ are the same, and simple binning seemed adequate to compute the joint distribution r_{ij}, so more sophisticated procedures[55,56] were not employed. Note that when $s_1=s_2$, the mutual information reduces to the single-point entropy, $I(0)=-\Sigma_i p_i \log_2 p_i$, while I vanishes if s_1 and s_2 are independent; that is, spatial localization implies that $I(l)\to 0$ as l becomes large.

The computed mutual information (independent of L) is shown in Fig. 11. Again, there is exponential decay, $I(l) \approx I(0)\exp(-l/\xi_I)$, where the mutual information correlation length $\xi_I \approx 3.8$. That is, the nonlinear correlations measured by the mutual information fall off more rapidly than the linear dependence captured by the autocorrelation function $C(x)$. The approximate relation $\xi_2 \approx 2\xi_I$ has been previously observed for the two-dimensional coupled map lattice Miller–Huse model.[53]

As Greenside[22] has pointed out, both ξ_2 and ξ_I may be unsatisfactory measures of STC, as they measure only spatial disorder, and are not dependent on time correlations of the spatial fields; changing the temporal ordering of the snapshots used to compute these correlation lengths would not affect $C(x)$ or $I(l)$. On dimensional grounds, a dimension correlation length ξ_δ has been proposed[21] as a more direct measure of dynamical complexity (see Ref. 22). Here, the motivation is the numerical observation (not yet supported by rigorous estimates in general) that the fractal dimension D_F of the STC attractor is extensive for the KS equation;[14] that is, asymptotically $D_F \propto L$. [In fact, Cross and Hohenberg (Ref. 21, p. 945) have proposed extensivity of D_F as a general defining feature of STC.] This suggests defining, for some measure of fractal dimension, a length by the inverse dimension density, or density of positive Lyapunov exponents, $\xi_\delta = \lim_{L\to\infty} L/D_F(L)$. From the results of Manneville[14] on the Lyapunov dimension of the KS equation (see Ref. 21, p. 951) we find $\xi_\delta \approx 4.35$. Note however that a quantity such as ξ_δ defined on purely dimensional considerations does not unambiguously imply a characteristic physical interaction length. Moreover, the definition of ξ_δ depends on extensivity and spatial localization, and thus does not provide independent support for these concepts.

Since a fractal dimension for a high-dimensional system is generally very difficult to compute, Zoldi and Greenside[57] have proposed replacing D_F by a Karhunen–Loève dimension $D_{\mathrm{KLD}}(f)$, defined by the number of eigenmodes in the proper orthogonal decomposition required to capture a given fraction f of the total energy; and have hence defined a Karhunen–Loève correlation length ξ_{KLD}. In the absence of an *a priori* choice for f, ξ_{KLD} is not quantitatively well-defined, however (we find $\xi_{\mathrm{KLD}} \approx 12.23$ for $f=0.5$). Furthermore, for a translationally invariant system such as the periodic KS equation (1), the Karhunen–Loève eigenmodes are Fourier modes,[2] so that ξ_{KLD} for any f can be computed directly[16] from the power spectrum $S(q)$, and thus contains no more dynamical information than ξ_2.

The correlation lengths discussed are all statistical averages, and might not capture short-time or rare events. Moreover (with the possible exception of ξ_δ), they are measures only of spatial disorder, without capturing any information on the temporally complex dynamics responsible for the disorder. In order to investigate the local nature of instantaneous spatiotemporal dynamics, we now propose an experiment to test the range of influences relevant to the short-time interactions (with the hope of gaining understanding of the ''microscopic'' basis of STC, and to aid in the construction of models). To do so, we need a means of manipulating instantaneous couplings, which can be achieved by solving the KS equation on a localized basis such as a wavelet basis.

C. A dynamical interaction distance: An experiment

In Sec. II, the wavelet decomposition of $u(x,t)$ was used to study scale and space localization through the temporal dynamics and distributions of wavelet coefficients $a_\alpha(t)$, as well as through a series of experiments elucidating the dynamical contributions of different wavelet levels. Similarly, we may perform numerical experiments exploiting the narrow spatial support of wavelets to analyze spatial localization of the KS dynamics more directly. To do this, we substitute the wavelet decomposition (4) into (1) to find the wavelet Galerkin projection of the KS equation,

$$\frac{d}{dt}a_\alpha(t)=\sum_{\alpha'} l_{\alpha\alpha'}a_{\alpha'}+\sum_{\alpha',\alpha''} n_{\alpha\alpha'\alpha''}a_{\alpha'}a_{\alpha''}, \tag{6}$$

where $l_{\alpha\alpha'}=-\int_0^L \psi_\alpha(\partial_{xx}\psi_{\alpha'}+\partial_{xxxx}\psi_{\alpha'})dx$, $n_{\alpha\alpha'\alpha''}=-\int_0^L \psi_\alpha\psi_{\alpha'}\partial_x\psi_{\alpha''}dx$, and α represents the multi-index (j,k).

Unlike the Fourier representation (2), the linear part of the wavelet Galerkin projection is not diagonal, as there is

overlap of wavelets both within a scale and across scales. However, due to the scale and space localization of the wavelet basis, this overlap is limited. For instance, $l_{\alpha\alpha'} = l_{jkj'k'}$ couples wavelets at scales j and j'; but due to the power law decrease of ψ in Fourier space, this decays with the scale separation $|j-j'|$. More importantly for the present purpose, we can define a distance between the centers x_α of wavelets ψ_α, $d_{\alpha\alpha'} = |x_\alpha - x_{\alpha'}|$; for wavelets at the same level, $d_{jkjk'} = L2^{-j}|k-k'|$. The linear term $l_{\alpha\alpha'}$ thus measures the overlap between wavelets (and their derivatives) centered a distance $d_{\alpha\alpha'}$ apart, and falls off exponentially from the diagonal[4,41] due to the spatial exponential decay of $\psi(x)$; similarly for the nonlinear term $n_{\alpha\alpha'\alpha''}$. That is, the evolution of a particular wavelet coefficient is affected primarily by those modes $a_{\alpha'}$ for which $(l_{\alpha\alpha'} + \Sigma_{\alpha''} n_{\alpha\alpha'\alpha''} a_{\alpha''}) a_{\alpha'}$ is appreciable, those centered near a_α in space.

We may use the above considerations to manipulate the KS dynamics and probe spatial localization. Since the coefficients $l_{\alpha\alpha'}$ and $n_{\alpha\alpha'\alpha''}$ in the Galerkin projection represent coupling between wavelets localized a distance $d_{\alpha\alpha'}$ or $d_{\alpha\alpha''}$ apart, we can cut all interactions beyond a certain length l_c by setting the corresponding coefficients to zero, leading to a localized model

$$\dot{a}_\alpha = \sum_{\alpha'} \tilde{l}_{\alpha\alpha'} a_{\alpha'} + \sum_{\alpha',\alpha''} \tilde{n}_{\alpha\alpha'\alpha''} a_{\alpha'} a_{\alpha''}, \tag{7}$$

where $\tilde{l}_{\alpha\alpha'} = l_{\alpha\alpha'}$ if $d_{\alpha\alpha'} \leqslant l_c$, $\tilde{l}_{\alpha\alpha'} = 0$ otherwise, and similarly for the nonlinear term. This allows us to quantify the *instantaneous* dynamical significance of the interaction length l_c.

Such calculations are computationally expensive: In contrast to rapid finite difference and pseudospectral schemes, the wavelet Galerkin method of (7) on N modes requires $\mathcal{O}(N^3)$ steps (and the storage of the N^3 terms of $n_{\alpha\alpha'\alpha''}$), while an enhancement using the fast wavelet transform still requires $\mathcal{O}(N^2 \log N)$ computations per time step. A consequence of this is that long-time calculations, for a range of values of l_c, are prohibitively expensive; whereas for short times, we cannot hope to obtain well-converged statistics for many of the quantities discussed previously.

We performed over 50 computations to time $t_{\max} \approx 1000$ with a range of interaction lengths l_c, for several different initial conditions and systems lengths L. Since the dynamics are so sensitive to initial conditions, we would need to perform many runs with different initial data for each set of parameter values to obtain conclusive results; thus our experiments should be regarded as preliminary.

In general, we find that if l_c is large enough, we recover the essential KS dynamics, while small l_c results in significant disruption; a departure from the typical events, and changes in space and time scales, and in the form of the coherent structures. Among the features we observe when the interaction length is sufficiently reduced are break-up into apparently independent subdomains, the presence of localized peaks, and fast local traveling pulses colliding with the peaks. Frequently there is an energy buildup at large scales, which are disproportionately excited relative to the full KS equation. This large-scale excitation often results in a rapid, spatially localized transfer of energy to the small scales, leading to numerical blowup; with decreasing l_c such blowup becomes more likely and typically occurs sooner. To counteract such rapid transfer across scales, we also performed some experiments in which we cut couplings across more than 3 wavelet scales, that is, for $|j-j'|>3$; this measure seems to prevent or delay numerical blowup. The disruption does not decrease monotonically with increasing l_c: we also encountered some relatively large values of l_c for which there was an unusual likelihood of blowup, or capture into a steady state; this is reminiscent of a ''resonance'' effect encountered when solving the KS equation on short subdomains in Fourier space projections.[58]

Some representative results for system length $L=100$ and different coupling lengths l_c are shown in Fig. 12. Note that $l_c = L/2 = 50$ is the maximum distance between two points in an $L=100$ periodic system, and thus corresponds to retaining all interactions; thus we have confirmed that our $l_c = 50$ wavelet calculation (not shown) reproduces the full KS dynamics. Figure 12(a) shows that for large enough l_c, we retain the characteristic KS dynamics (see Fig. 1). As we decrease l_c, many typical features remain, but the dynamics become increasingly disrupted, with rigid peaks, traveling pulses and excitation of the large scales [Figs. 12(b) and 12(c)]. Numerical blowup becomes increasingly likely for sufficiently small l_c [Fig. 12(d)].

The conclusions of visual inspections are supported by the energy distributions across wavelet levels (Fig. 13), for the same values of l_c, compared to the spectrum for the full KS equation (Fig. 4). As l_c decreases, the energy goes increasingly to larger scales (lower j). In this light, we can consider a (phenomenological) measure of the extent of disruption of the dynamics, the energy transfer to large scales. Specifically, in Fig. 14(a) we plot e_2/e_4, where $j=4$ is the most active wavelet level for the full KS equation.

These and related considerations for a range of experiments, including ones with varying L discussed below, lead us to estimate a typical interaction length $\overline{l_c}$, beyond which cutting interactions significantly disrupts the KS dynamics; from Fig. 14(a), this is $\overline{l_c} \approx 25$. We interpret this length so that for $l_c > \overline{l_c}$, we typically obtain characteristic KS dynamics, improving as l_c approaches $L/2$, while the dynamics are increasingly disrupted as l_c decreases below $\overline{l_c}$. To our knowledge, this is the first attempt to quantify the *dynamical* significance of a coupling distance, in terms of its effect on the temporal evolution.

We note that the effect of cutting interactions is strongly dependent on the dyadic structure of the wavelet decomposition. That is, which modes interact for a given l_c depends discontinuously on l_c. For instance, for $L=100$, $l_c \geqslant 25$, adjacent wavelets at level $j=2$ are coupled, while they cease to interact for $l_c < 25$. This experiment is therefore a rather crude measure of interaction length, which may depend on the decomposition as well as the dynamics. To confirm that l_c is indeed a relevant interaction length, we performed some experiments for $L=200$ (which effectively corresponds to a shift by one wavelet level); even though many more wavelet

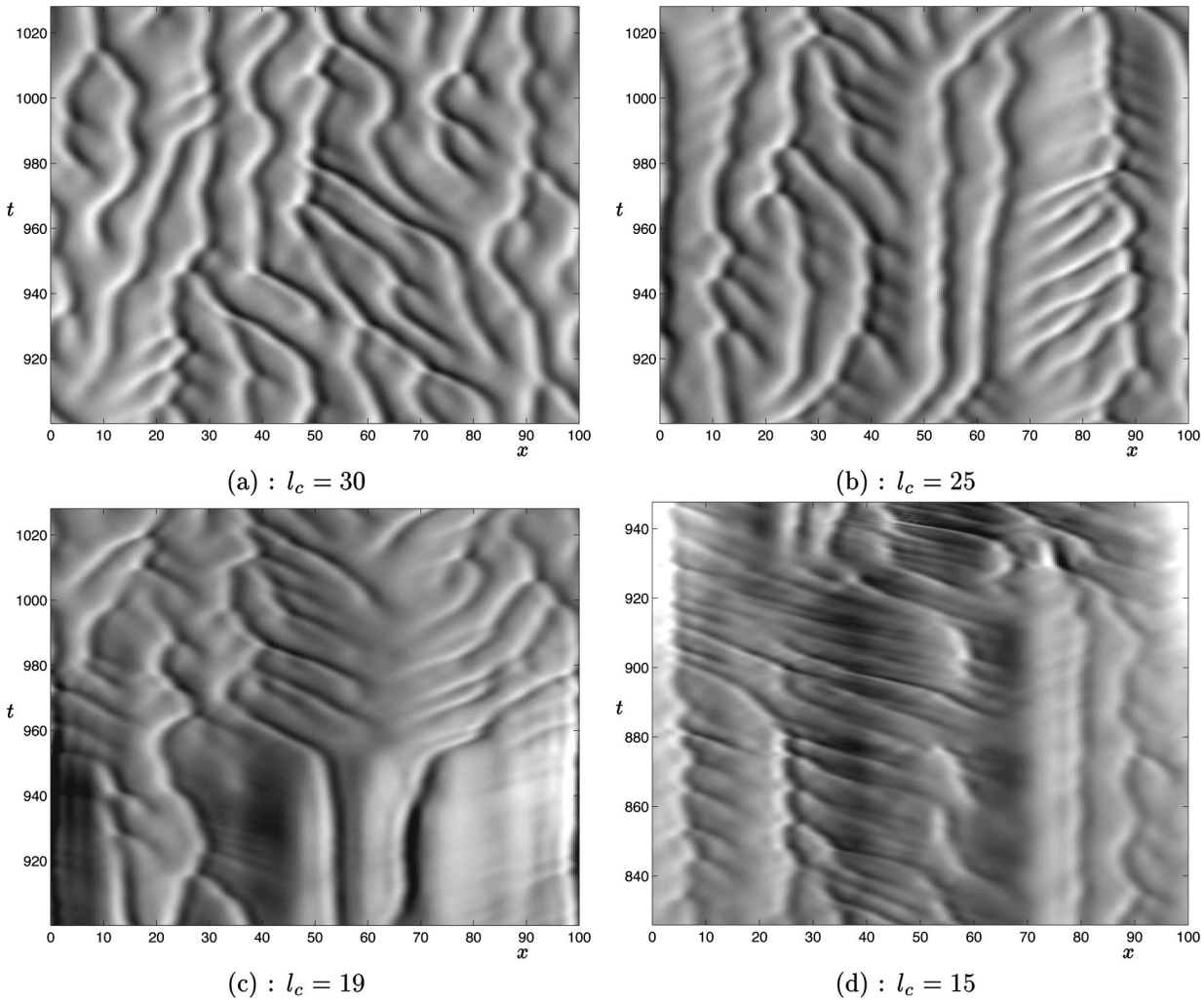

FIG. 12. Modified KS equation (7), coupling only wavelets nearer than l_c apart, for $L=100$, and $N=127$ wavelets; note the increasing disruption of KS dynamics as l_c decreases: (a) $l_c=30$; (b) $l_c=25$; (c) $l_c=19$; (d) $l_c=15$, just before blowup. Note: vertical scales are expanded in comparison with Fig. 1.

interactions are cut, the results for a given l_c agree with those for $L=100$. Similarly, we repeated the calculations for $L=80$ and $L=128$, which have a different relationship of intrinsic length to the dyadic decomposition, and confirmed that although the distribution of energy among the wavelet levels influences the experimental results, $\overline{l_c}\approx 25$ still appears to be a relevant interaction length; see Figs. 14(b) and 14(c).

The interaction distance we have defined measures the distance between the centers of wavelets. Due to the finite support of $\psi(x)$, the value of $\overline{l_c}$ is only an approximation to the spatial range of interactions: there may be appreciable overlap between wavelets centered more than l_c apart. For this reason, the wavelet approach only yields a fairly rough estimate of spatial localization. However, the wavelets we use are exponentially localized in x, so the effect of noncompact wavelets is limited.

The dynamical interaction distance l_c estimated by this technique, appears to be considerably larger than the mutual information distance $\xi_I\approx 3.8$, or the autocorrelation distance $\xi_2\approx 7.4$. These other lengths are obtained from time averaging over the dynamics. The results $\overline{l_c}>\xi_I$, for instance, may indicate that the dynamics are strongly influenced by rare events which couple relatively distant spatial locations (separated by more than one cell). Thus, statistically averaged lengths such as ξ_I may be underestimates of the dynamically relevant coupling distance; the asymptotic mutual statistical independence of two points is insufficient to imply their instantaneous dynamical independence.

Our results indicate that in a successful low-dimensional

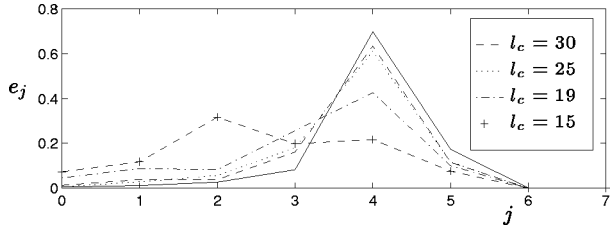

FIG. 13. Wavelet energy distributions, for $L=100$ and coupling lengths l_c as in Fig. 12; the solid line is the distribution for the full KS equation, from Fig. 4.

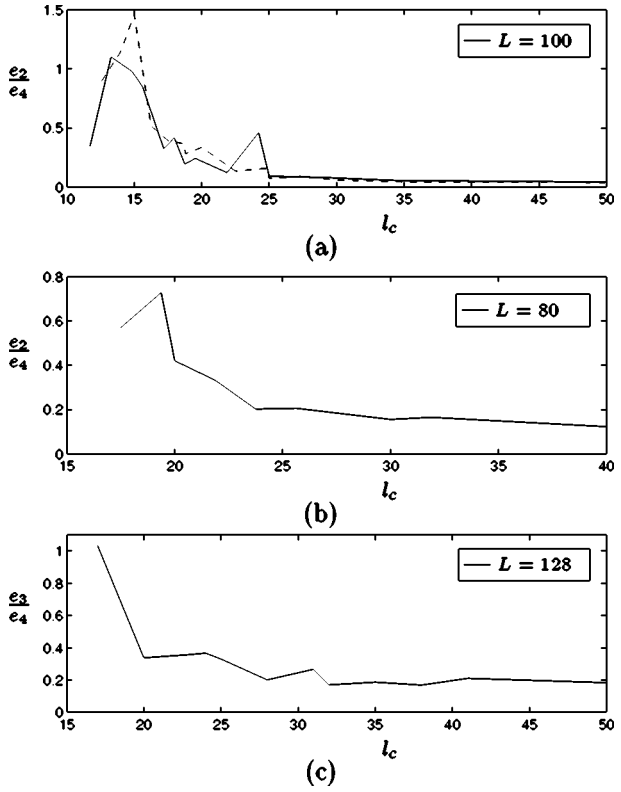

FIG. 14. Energy ratio, a diagnostic for energy transfer as a function of interaction length l_c. (a) e_2/e_4 for $L=100$: computations for two different initial conditions; (b) e_2/e_4 for $L=80$; (c) e_3/e_4 for $L=128$. The ratios appear to settle down to their asymptotic values for $l_c \geqslant \overline{l_c} \approx 25$. These curves exclude computations for which blowup occurred before $t=128$.

''short'' model for the KS dynamics, wavelets should be coupled, either to other modes or to external forcing, up to at least a distance $\sim \overline{l_c}$, to ensure sufficient interactions. We shall report on the construction of such models elsewhere.[59]

This work also helps us to understand the transition to STC in the KS equation. For $L \leqslant 2\overline{l_c} \approx 50$, spatial locations are ''doubly'' coupled (due to periodicity); that is, for a given x_0 and interaction distance $l \leqslant \overline{l_c}$, x_0 is coupled to $x_0 + l$ and $x_0 - l (\mathrm{mod}\, L)$, which could be the same point. Small systems are thus excessively constrained through their interactions, and consequently solutions frequently approach a ''simple'' attractor. For systems of length greater than about 50 or 60, on the other hand, x_0 is asymptotically and dynamically independent of $x_0 \pm L/2$, there are fewer constraints, and the system can sustain STC behavior.

IV. DISCUSSION

We have confirmed the localization of KS dynamics in scale and space, not merely in terms of averaged distributions and asymptotic linear or nonlinear correlations, but also in terms of the dynamic relevance of different modes. Our results provide strong evidence in addition to the existing literature on the separation of scales and space localization of the dynamics in a spatiotemporally chaotic system. In particular, for large lengths L, the statistics can be understood in terms of local events; and the results are consistent with the picture of weakly interacting small subsystems and extensivity. Spatial localization implies that the statistics are essentially invariant for $L \geqslant 50$, while for shorter lengths, the periodic boundary conditions constrain the dynamics, so that chaos can typically not be maintained, and there are ''simple'' attractors. A suitably chosen wavelet basis clearly helps one extract interesting features of the dynamics, which remain obscured in real and Fourier space representations.

In addition to clarifying the nature of STC in the KS equation, our results aid the construction of low-dimensional models of the spatiotemporal dynamics, by providing a range of quantitative measures with which to assess the validity of models by comparison with the full equation; for instance, the statistics of time scales and distributions at different scales provide more detailed diagnostics than the global power spectrum. The spatial interaction length $\overline{l_c}$ provides a limit on how much one may expect to restrict spatial interactions without disrupting the dynamics excessively, and hence how small a system one can use. Moreover, for wavelet-based models in particular,[4,41] Sec. II reveals the types of forcing needed to feed in to represent neglected modes in a low-dimensional model; in particular, the distributions and temporal correlations are strongly scale-dependent. This leads to construction of families of ''short'' local models; wavelet Galerkin projections forced by colored Gaussian noise to reproduce excluded large scales, and periodized to replace the active scale dynamics of spatial neighbors. These models will be described elsewhere.[59]

ACKNOWLEDGMENTS

R.W.W. would like to thank J. Elezgaray for providing his computer code for some of the wavelet transform calculations, and J. Elezgaray, H. Greenside, E. Titi, and D. W. McLaughlin for useful discussions. This work was partially supported by DOE Grant No. DE-FG02-95ER25238 and by a Charlotte Elizabeth Procter Fellowship at Princeton University.

[1] N. Aubry, P. Holmes, J. L. Lumley, and E. Stone, J. Fluid Mech. **192**, 115 (1988).
[2] P. Holmes, J. L. Lumley, and G. Berkooz, *Turbulence, Coherent Structures, Dynamical Systems and Symmetry* (Cambridge University Press, Cambridge, 1996).
[3] P. J. Holmes, J. L. Lumley, G. Berkooz, J. C. Mattingly, and R. W. Wittenberg, Phys. Rep. **287**, 337 (1997).
[4] G. Berkooz, J. Elezgaray, and P. Holmes, Physica D **61**, 47 (1992).
[5] J. Elezgaray, G. Berkooz, and P. Holmes, in *Progress in Wavelet Analysis and Applications*, edited by Y. Meyer and S. Roques (Editions Frontieres, Gif-sur-Yvette, 1993), pp. 471–476.
[6] M. Myers, P. Holmes, J. Elezgaray, and G. Berkooz, Physica D **86**, 396 (1995).
[7] R. LaQuey, S. Mahajan, P. Rutherford, and W. Tang, Phys. Rev. Lett. **34**, 391 (1975).
[8] B. Cohen, J. Krommes, W. Tang, and M. Rosenbluth, Nucl. Fusion **16**, 971 (1976).
[9] Y. Kuramoto and T. Tsuzuki, Prog. Theor. Phys. **55**, 356 (1976).
[10] Y. Kuramoto, *Chemical Oscillations, Waves, and Turbulence*, Vol. 19 in *Springer Series in Synergetics* (Springer, Berlin Heidelberg, 1984).
[11] G. Sivashinsky, Acta Astron. **4**, 1177 (1977).
[12] G. Sivashinsky and D. Michelson, Prog. Theor. Phys. **63**, 2112 (1980).
[13] C. Misbah and A. Valance, Phys. Rev. E **49**, 166 (1994).
[14] P. Manneville, in *Macroscopic Modelling of Turbulent Flows*, Vol. 230 of *Lecture Notes in Physics*, edited by U. Frisch, J. Keller, G. Papanicolaou, and O. Pironneau (Springer, Berlin Heidelberg, 1985), pp. 319–326.
[15] A. Pumir, J. Phys. (France) **46**, 511 (1985).

[16] R. W. Wittenberg, Ph.D. thesis, Princeton University, 1998.
[17] J. M. Hyman and B. Nicolaenko, Physica D **18**, 113 (1986).
[18] J. M. Hyman, B. Nicolaenko, and S. Zaleski, Physica D **23**, 265 (1986).
[19] I. G. Kevrekidis, B. Nicolaenko, and J. C. Scovel, SIAM J. Appl. Math. **50**, 760 (1990).
[20] D. Armbruster, J. Guckenheimer, and P. Holmes, SIAM J. Appl. Math. **49**, 676 (1989).
[21] M. Cross and P. Hohenberg, Rev. Mod. Phys. **65**, 851 (1993).
[22] H. S. Greenside, in *Semianalytic Methods for the Navier–Stokes Equations*, in *Proceedings of the CRM Workshop*, edited by K. Coughlin (Centre de Recherches Mathématiques, Montréal, 1998).
[23] L. Landau and E. Lifshitz, *Statistical Physics*, Part 1, Vol. 5 in *Course of Theoretical Physics*, 3rd ed. (Pergamon, Oxford, 1980).
[24] D. Michelson, Physica D **19**, 89 (1986).
[25] Z. Grujić, J. Dynam. Diff. Eq. (to be published).
[26] P. Collet, J.-P. Eckmann, H. Epstein, and J. Stubbe, Commun. Math. Phys. **152**, 203 (1993).
[27] P. Collet, J.-P. Eckmann, H. Epstein, and J. Stubbe, Physica D **67**, 321 (1993).
[28] Z. Grujić and I. Kukavica, J. Funct. Anal. **152**, 447 (1998).
[29] Z. Grujić and I. Kukavica, preprint, 1997.
[30] H. Fujisaka and T. Yamada, Prog. Theor. Phys. **57**, 734 (1977).
[31] Y. Pomeau, A. Pumir, and P. Pelce, J. Stat. Phys. **37**, 39 (1984).
[32] S. Toh, J. Phys. Soc. Jpn. **56**, 949 (1987).
[33] V. Yakhot, Phys. Rev. A **24**, 642 (1981).
[34] M. Kardar, G. Parisi, and Y.-C. Zhang, Phys. Rev. Lett. **56**, 889 (1986).
[35] J. Krug and H. Spohn, in *Solids Far From Equilibrium*, Vol. 1 in *Monographs and Texts in Statistical Physics*, edited by C. Godrèche (Cambridge University Press, Cambridge, 1991), Chap. 6, pp. 479–582.
[36] K. Sneppen, J. Krug, M. H. Jensen, C. Jayaprakash, and T. Bohr, Phys. Rev. A **46**, R7351 (1992).
[37] V. S. L'vov, V. V. Lebedev, M. Paton, and I. Procaccia, Nonlinearity **6**, 25 (1993).
[38] C. C. Chow and T. Hwa, Physica D **84**, 494 (1995).
[39] I. Daubechies, *Ten Lectures on Wavelets*, Vol. 61 in *CBMS-NSF Regional Conference Series in Applied Mathematics* (SIAM, Philadelphia, 1992).
[40] M. Farge, Annu. Rev. Fluid Mech. **40**, 395 (1992).
[41] J. Elezgaray, G. Berkooz, and P. Holmes, Phys. Rev. E **54**, 224 (1996).
[42] V. Perrier and C. Basdevant, Rech. Aerosp. **1989-3**, 53 (1989).
[43] D. Forster, D. R. Nelson, and M. J. Stephen, Phys. Rev. A **16**, 732 (1977).
[44] F. Hayot, C. Jayaprakash, and C. Josserand, Phys. Rev. E **47**, 911 (1993).
[45] U. Frisch, *Turbulence: The Legacy of A. N. Kolmogorov* (Cambridge University Press, Cambridge, 1995).
[46] R. H. Kraichnan, Phys. Rev. Lett. **65**, 575 (1990).
[47] R. Benzi, L. Biferale, G. Paladin, A. Vulpiani, and M. Vergassola, Phys. Rev. Lett. **67**, 2299 (1991).
[48] U. Frisch and R. Morf, Phys. Rev. A **23**, 2673 (1981).
[49] G. L. Browning, W. D. Henshaw, and H.-O. Kreiss, preprint, April, 1998; UCLA CAM Report No. 98-23 (unpublished).
[50] U. Frisch, Z. S. She, and O. Thual, J. Fluid Mech. **168**, 221 (1986).
[51] D. A. Egolf and H. S. Greenside, Phys. Lett. A **185**, 395 (1994).
[52] S. Zaleski and P. Lallemand, J. Phys. (France) Lett. **46**, L793 (1985).
[53] C. S. O'Hern, D. A. Egolf, and H. S. Greenside, Phys. Rev. E **53**, 3374 (1996).
[54] A. Papoulis, *Probability, Random Variables, and Stochastic Processes*, 2nd ed. (McGraw–Hill, New York, 1984).
[55] A. M. Fraser, IEEE Trans. Inf. Theory **35**, 245 (1989).
[56] A. M. Fraser and H. L. Swinney, Phys. Rev. A **33**, 1134 (1986).
[57] S. M. Zoldi and H. S. Greenside, Phys. Rev. Lett. **78**, 1687 (1997).
[58] H. Dankowicz, P. Holmes, G. Berkooz, and J. Elezgaray, Physica D **90**, 387 (1996).
[59] R. W. Wittenberg and P. Holmes (submitted, 1999).